Photocarrier recombination dynamics in highly excited $SrTiO_3$ studied by transient absorption and photoluminescence spectroscopy

Yasuhiro Yamada,[1] Hideki Yasuda,[1] Takeshi Tayagaki,[1] and Yoshihiko Kanemitsu[1,2,a)]
[1]*Institute for Chemical Research, Kyoto University, Uji, Kyoto 611-0011, Japan*
[2]*Photonics and Electronics Science and Engineering Center, Kyoto University, Kyoto 615-8510, Japan*

(Received 3 August 2009; accepted 5 September 2009; published online 25 September 2009)

We studied photocarrier recombination processes in highly excited $SrTiO_3$ crystals using pump-probe transient absorption (TA) and photoluminescence (PL) spectroscopy at room temperature. TA signals of nondoped $SrTiO_3$ crystals clearly appear in the visible and infrared spectral region under intense interband photoexcitation, and TA spectra show Drude-like photon-energy dependence. Both TA and PL decay curves are well explained by the same simple rate equation including three-body Auger recombination and single-carrier trapping. © *2009 American Institute of Physics*. [doi:10.1063/1.3238269]

Over the past decade, perovskite oxides and their heterostructures have attracted a great deal of attention as unique device materials because they have a wide variety of fascinating and multifunctional properties.[1,2] Among perovskite oxides, $SrTiO_3$ has been regarded as one of the most important materials because $SrTiO_3$ has been widely used as a substrate material for transparent oxide electronics. In addition, by electron doping, $SrTiO_3$ itself shows multifunctional electrical properties ranging from insulating to semiconducting, metallic, and superconducting.[3–5] The interest to $SrTiO_3$ is further increased by unique electronic and magnetic properties of two-dimensional electron gases formed at the interfaces between $SrTiO_3$ and other oxides.[6–9] Despite extensive studies of electronic structures and electrical properties of $SrTiO_3$ and related heterostructures, the carrier dynamics that determines electronic and optical properties remains unclear even in $SrTiO_3$ bulk crystals. Impurities and defects in $SrTiO_3$ crystals affect optical responses and the carrier recombination dynamics,[10,11] and thus there have been so far no quantitative discussions on intrinsic carrier recombination processes.

Recent discovery of the blue photoluminescence (PL) in $SrTiO_3$ provides a chance to deep understanding of carrier dynamics and electronic properties of $SrTiO_3$ crystals and $SrTiO_3$ based heterostructures.[12,13] Broad blue PL at around 2.9 eV was reported in electron-doped $SrTiO_3$ (Ar^+-irradiated $SrTiO_3$) at room temperature,[12] and similar blue PL was observed in nondoped $SrTiO_3$ under intense photoexcitation.[13] Under intense photoexcitation, defect and impurity PL usually saturates, and intrinsic carrier recombination processes appear and determine the room-temperature blue PL dynamics.[14] Thus, we anticipate that blue PL spectrum and lifetime are used as a probe for determining spatial profiles of carriers and defects.[15] Study of the carrier dynamics by different evaluation methods is essential for understanding of the PL origins in $SrTiO_3$ and for quantitative characterization of $SrTiO_3$ thin films and heterostructures.

In this letter, we performed transient absorption (TA) and PL measurements in nondoped $SrTiO_3$ crystals under intense photoexcitation at room temperature. TA spectra in nondoped $SrTiO_3$ crystals are similar to linear absorption spectra of electron-doped $SrTiO_3$ crystals, originating from doped carriers in the samples. The carrier recombination dynamics evaluated from TA and PL experiments is well explained by a simple model involving the nonlinear Auger recombination and single-carrier trapping processes. From the analysis of the carrier decay times, we determine Auger recombination and single-carrier trapping coefficients.

We used nondoped $SrTiO_3$ and electron-doped $SrTi_{1-x}Nb_xO_3$ (Nb-doped $SrTiO_3$) single crystals with several dopant concentrations (commercially available from Furuuchi Chemical Co.). Nondoped samples were annealed under oxygen flow for 24 h at 700 K to reduce oxygen vacancies. The samples were 0.5 mm thick. Time-resolved PL and TA measurements were performed using an optical parametric amplifier system based on a regenerative amplified mode-locked Ti:sapphire laser with a pulse duration of 150 fs and a repetition rate of 1 kHz. The excitation photon energy was 3.49 eV. The laser spot size on the sample surface was measured carefully using the knife-edge method. The femtosecond time-resolved TA measurements were performed by using a pump-probe technique. An aperture with 10 μm diameter was attached on the sample surface to ensure the homogeneous excitation laser intensity and the overlap of the pump and probe pulses. In temporal profile measurements, the photon energy of the probe pulse was 1.55 eV and a photodiode with a lock-in amplifier was used for detection. In TA spectral measurements, we used white light as a probe pulse obtained by focusing 1.55 eV laser pulse on the sapphire plate, and used a charge coupled device and an InGaAs diode array for detection. We also measured TA decay curves in the nanosecond time region using a photodiode and a digital oscilloscope. The probe light source was a continuous-wave diode laser whose photon energy was 1.57 eV and the time resolution of this experimental setup was approximately 2 ns. In time-resolved PL measurements, we used a streak camera and a monochromator, where the time resolution of our setup was 40 ps. All measurements were performed at room temperature. While the PL intensity is determined by the product of the electron and hole densities, the intraband TA signal directly reflects the electron or hole density. From both TA and PL measurements, we discuss

a)Author to whom correspondence should be addressed. Electronic mail: kanemitu@scl.kyoto-u.ac.jp.

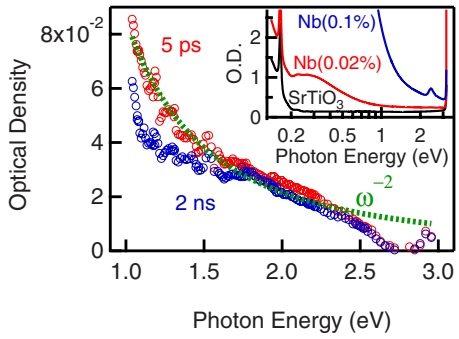

FIG. 1. (Color online) TA spectra at the delay times of 5 ps and 2 ns. Drude-like ω^{-2} curve is shown for guide to the eye. The inset shows the linear absorption spectra of nondoped $SrTiO_3$, and Nb-doped $SrTiO_3$ (0.02 and 0.1 mol %).

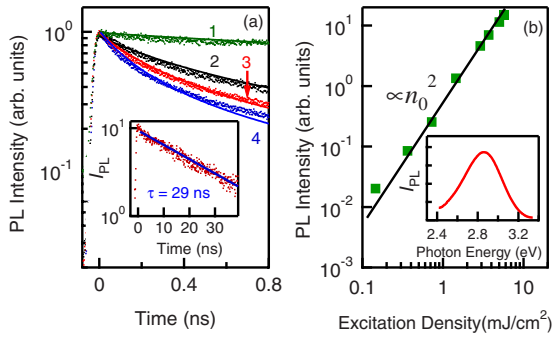

FIG. 3. (Color online) (a) PL decay dynamics under excitation of (1) 1.5 mJ/cm^2, (2) 3.8 mJ/cm^2, (3) 5.2 mJ/cm^2, and (4) 5.9 mJ/cm^2 in the subnanosecond time region. The inset shows the PL decay dynamics under excitation of 0.4 mJ/cm^2. (b) The excitation density dependence of the PL intensity just after excitation. The inset shows a typical PL spectrum of $SrTiO_3$.

photocarrier decay dynamics in highly excited $SrTiO_3$ in more detail.

The inset of Fig. 1 shows the linear absorption spectra of nondoped $SrTiO_3$ and electron-doped $SrTiO_3$ (Nb-doped $SrTiO_3$) with several doping concentrations. In nondoped $SrTiO_3$, there is no optical absorption below the band gap of 3.2 eV in the visible region. The 0.16 eV peak is assigned to an electronic transition of the defects.[16] On the other hand, electron-doped $SrTiO_3$ shows a Drude-like broad absorption band in the visible and infrared region. The spectrum shape of electron doped $SrTiO_3$ is dependent on the doped carrier density. The relatively narrow 2.4 eV band is assigned to optical transition from a deep impurity level to the conduction band.[16]

Figure 1 shows TA spectra of nondoped $SrTiO_3$ at the delay times of 5 ps and 2 ns under 1.0 mJ/cm^2 excitation. Just after laser excitation, a broad TA band appears in the infrared and visible region blow the band-gap energy. The spectral shapes at 5 ps and 2 ns time delays are almost the same with each other. TA spectra of highly excited $SrTiO_3$ show Drude-like ω^{-2} dependence and are similar to linear absorption spectra of electron-doped $SrTiO_3$. This indicates that the photoinduced TA spectra in highly excited $SrTiO_3$ results from intraband optical transitions of photogenerated carriers.

Figure 2 shows temporal changes in TA signals at different excitation densities of 0.5, 4.4, 8.9, and 13.3 mJ/cm^2. Since the broad TA band has no fine structures in the range

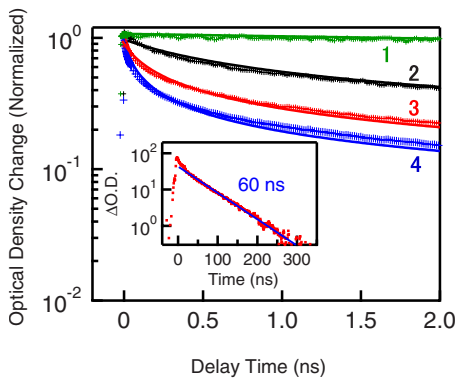

FIG. 2. (Color online) TA decay dynamics of nondoped $SrTiO_3$ at different excitation densities of (1) 0.5 mJ/cm^2, (2) 4.4 mJ/cm^2, (3) 8.9 mJ/cm^2, and (4) 13.3 mJ/cm^2. The inset shows the temporal evolution of optical density change (ΔOD) at 0.8 mJ/cm^2 excitation density in the nanosecond time region.

of 1–2 eV, we used the 1.55 eV laser as a probe pulse for temporal changes of the carrier density. Under weak excitation of 0.5 mJ/cm^2, the TA signal shows very slow decay and the decay time is much longer than 2 ns. As shown in the inset of Fig. 2, the TA signal shows a single exponential decay with a decay time of 60 ns under the weak excitation condition of 0.8 mJ/cm^2. Under high excitation densities above about 3 mJ/cm^2, the fast and nonexponential decay component clearly appears in the subnanosecond time region, and the TA decay time becomes faster as increasing the excitation density.

We also studied the PL decay dynamics of nondoped $SrTiO_3$ for comparison with TA studies under the same experimental conditions. Figure 3(a) shows PL decay curves of nondoped $SrTiO_3$ in the subnanosecond time region under excitation densities of 1.5, 3.8, 5.2, and 5.9 mJ/cm^2. The monitored PL photon energy was 2.9 eV, which is the peak energy of the broad PL spectrum as shown in the inset of Fig. 3(b). Under low excitation density, the PL dynamics shows slow decay. As shown in the inset of Fig. 3(a), the PL decay dynamics shows almost single exponential decay with the decay time of 29 ns under weak excitation density of 0.4 mJ/cm^2. As increasing the excitation density, fast and nonexponential decay component appears, and the PL decay time becomes shorter. These PL decay behaviors are quite similar to TA decay ones. Figure 3(b) shows the excitation-intensity dependence of the PL intensity just after excitation: I_0. The PL intensity shows quadratic dependence on the excitation density. This means that the blue PL originates from the two-body (bimolecular) recombination of photocarriers, because excitonic states are unstable due to the large dielectric constant ($\varepsilon \sim 300$ at 300 K).[17]

The excitation-density dependence of the TA and PL decay times is summarized in Fig. 4. Here, we define the effective decay time $t_{1/e}$ as the time at the carrier density of n_0/e. The initial photogenerated carrier density n_0 is estimated from the incident photon number and the optical absorption coefficient at the excitation photon energy in Ref. 18. Note that $I_{PL}(t_{1/e})=I_{PL}(0)/e^2$ and $\alpha_{TA}(t_{1/e})=\alpha_{TA}(0)/e$ are used because of the relations $I_{PL} \propto n^2$ and $\alpha_{TA} \propto n$, where I_{PL} and α_{TA} are the PL and TA densities. We plot $t_{1/e}$ derived from PL (denoted by circle) and TA (square) decay curves as a function of the excitation density in Fig. 4. The effective decay times $t_{1/e}$ of TA and PL signals show good accordance

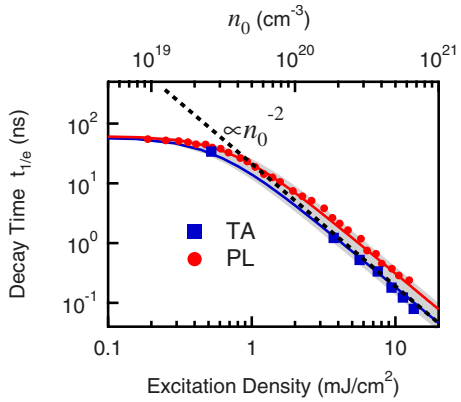

FIG. 4. (Color online) Excitation-density dependence of the decay times $t_{1/e}$ derived from TA and PL decay curves. The solid curves show the fitting results using Eq. (2).

with each other. Below about 0.5 mJ/cm^2, $t_{1/e}$ is independent of the excitation density, while it decreases as the inverse square of the excitation density under high excitation densities. This indicates that the carrier dynamics is dominated by three-body processes, such as Auger recombination process, under high intensity excitation.

Here, we discuss the carrier dynamics in highly photoexcited $SrTiO_3$ using the rate equation of photocarriers. In semiconductors, the rate equation for the photocarriers can be simplified and written as follows:[13,19]

$$\frac{dn}{dt} = -An - Bn^2 - Cn^3, \tag{1}$$

where n is the photocarrier density. An represents the single-carrier trapping. Bn^2 consists of bimolecular radiative recombination process and nonradiative trap-Auger recombination process.[19,20] Cn^3 represents the band-to-band (intrinsic) Auger recombination process, involving electron-electron-hole or electron-hole-hole processes, where the nonradiative recombination energy of the electron-hole pairs is transferred to the kinetic energy of the other electron (hole). According to Eq. (1), the effective decay time $t_{1/e}$ is approximately written as

$$t_{1/e} = (A + Bn_0 + Cn_0^2)^{-1}. \tag{2}$$

We fit the decay times of TA and PL dynamics shown in Fig. 4 by using Eq. (2). The best fit-parameters are $A=1.7\times10^7$ s^{-1} and $C=1.7\times10^{-32}$ cm^6 s^{-1} for TA dynamics, and $A=1.7\times10^7$ s^{-1} and $C=1.2\times10^{-32}$ cm^6 s^{-1} for PL dynamics. Here, we confirm that Bn^2 is negligibly small compared to An and Cn^3. In fact, the solid calculated curves shown in the Fig. 4 ($B=0$) reproduce the experimental results very well. This result means that the recombination rate of two-body processes (i.e., the radiative bimolecular recombination and trap Auger recombination) is very small in $SrTiO_3$. This result is consistent with the low PL quantum efficiency (PL quantum efficiency <0.01). The calculated TA and PL decay curves using the above best-fit-parameters also reproduce the experimental decay curves as shown in Figs. 2 and 3(a). From the TA and PL measurements and the calculation using the same equation, we determine the coefficients, $A=1.7\times10^7$ s^{-1} and $C=(1.5\pm0.3)\times10^{-32}$ cm^6 s^{-1}. No difference between TA and PL decay times clearly shows that the intrinsic Auger recombination process determines the photocarrier decay dynamics under high excitation density. The microscopic carrier recombination mechanisms determining A and C coefficients remain an open question.

In conclusion, we studied TA and PL decay dynamics in highly excited $SrTiO_3$ at room temperature. Both PL and TA decay curves are well explained by the same rate equation. We analyzed the excitation-density dependence of the TA and PL decay times and determined single-carrier trapping and Auger recombination coefficients.

Part of this work was supported by a Grant-in-Aid for Scientific Research on Innovative Area "Optical Science of Dynamically Correlated Electrons" (Grant No. 20104006) from MEXT, Japan.

[1] M. Imada, A. Fujimori, and Y. Tokura, Rev. Mod. Phys. **70**, 1039 (1998).
[2] W. Eerenstein, N. D. Mathur, and J. F. Scott, Nature (London) **442**, 759 (2006).
[3] J. F. Schooley, W. R. Hosler, and M. L. Cohen, Phys. Rev. Lett. **12**, 474 (1964).
[4] H. P. R. Frederikse, W. R. Thurber, and W. R. Hosler, Phys. Rev. **134**, A442 (1964).
[5] O. N. Tufte and P. W. Chapman, Phys. Rev. **155**, 796 (1967).
[6] A. Ohtomo and H. Y. Hwang, Nature (London) **427**, 423 (2004).
[7] A. Tsukazaki, A. Ohtomo, T. Kita, Y. Ohno, H. Ohno, and M. Kawasaki, Science **315**, 1388 (2007).
[8] G. Herranz, M. Basletic, M. Bibes, C. Carrétéro, E. Tafra, E. Jacquet, K. Bouzehouane, C. Deranlot, A. Hamzić, J. M. Broto, A. Barthélémy, and A. Fert, Phys. Rev. Lett. **98**, 216803 (2007).
[9] N. Reyren, S. Thiel, A. D. Caviglia, L. Koukoutis, G. Hammerl, C. Richter, C. W. Schneider, T. Kopp, A. S. Rüetschi, D. Jaccard, M. Gabay, D. A. Muller, J. M. Triscone, and J. Mannhart, Science **317**, 1196 (2007).
[10] T. Feng, Phys. Rev. B **25**, 627 (1982).
[11] S. Mochizuki, F. Fujishiro, and S. Minami, J. Phys.: Condens. Matter **17**, 923 (2005).
[12] D. Kan, T. Terashima, R. Kanda, A. Masuno, K. Tanaka, S. Chu, H. Kan, A. Ishizumi, Y. Kanemitsu, Y. Shimakawa, and M. Takano, Nature Mater. **4**, 816 (2005).
[13] H. Yasuda and Y. Kanemitsu, Phys. Rev. B **77**, 193202 (2008).
[14] Y. Yamada, H. Yasuda, T. Tayagaki, and Y. Kanemitsu, Phys. Rev. Lett. **102**, 247401 (2009).
[15] H. Yasuda, Y. Yamada, T. Tayagaki, and Y. Kanemitsu, Phys. Rev. B **78**, 233202 (2008).
[16] P. Rochon, J. L. Brebner, and D. Matz, Solid State Commun. **29**, 63 (1979).
[17] K. A. Muller and H. Burkard, Phys. Rev. B **19**, 3593 (1979).
[18] M. Cardona, Phys. Rev. **140**, A651 (1965).
[19] P. T. Landsberg, *Recombination in Semiconductors* (Cambridge University Press, Cambridge, 1991).
[20] P. T. Landsberg, Appl. Phys. Lett. **50**, 745 (1987).